Astrophysical searches for axions

Francesca Day

University of Cambridge

Quantum Connections 5
Axions in Stockholm - Reloaded
November 2018

Outline

Interactions

$$\mathcal{L} = \frac{1}{2}\partial_\mu a \partial^\mu a - \frac{1}{2} m_a^2 a^2 + g_{agg} a G \tilde{G} - \frac{g_{a\gamma\gamma}}{4} a F \tilde{F} + g_{aff} \overline{\Psi}_f \gamma^\mu \gamma_5 \Psi_f \partial_\mu a$$

- $g \sim \frac{1}{f_a}$
- QCD axion: $m_a f_a = m_\pi f_\pi$
- String ALP: m_a and f_a are free parameters.

Why astrophysics?

We know $f_a \gtrsim 10^{10}\,\mathrm{GeV}$. To detect such small couplings, we can:

- Measure things very carefully
- Exploit resonance
- Arrange for very big numbers

Axion production

Space produces a lot of axions:

Axion production

Space produces a lot of axions:

- Primordial production

Axion production

Space produces a lot of axions:

- Primordial production
- Production in stars

Axion production

Space produces a lot of axions:

- Primordial production
- Production in stars
- Black hole superradiance

Axion production

Space produces a lot of axions:

- Primordial production
- Production in stars
- Black hole superradiance
- Photon to axion conversion

Axion production

Space produces a lot of axions:

- Primordial production
- Production in stars
- Black hole superradiance
- Photon to axion conversion

We can detect:

Axion production

Space produces a lot of axions:

- Primordial production
- Production in stars
- Black hole superradiance
- Photon to axion conversion

We can detect:

- Axion to photon conversion or decay

Axion production

Space produces a lot of axions:

- Primordial production
- Production in stars
- Black hole superradiance
- Photon to axion conversion

We can detect:

- Axion to photon conversion or decay
- The absence of the energy source for axion production

Axion production

Space produces a lot of axions:

- Primordial production
- Production in stars
- Black hole superradiance
- Photon to axion conversion

We can detect:

- Axion to photon conversion or decay
- The absence of the energy source for axion production
- Gravitational effects

Primordial axion production

Axions may be produced in the early universe by:

- Particle decay (dark radiation)

Primordial axion production

Axions may be produced in the early universe by:

- Particle decay (dark radiation)
- Misalignment production (dark matter and dark energy):

$U(1)_A$ symmetry spontaneously broken. Massless axion field created.

$\downarrow$

Axion follows random walk in field space.

$\downarrow$

Non-perturbative effects generate axion mass. Axion field is now displaced from its minimum.

(See Jens' talk)

Axion Dark Matter

- Coherently oscillating scalar field: $\ddot{a} + 3H\dot{a} + m_a^2 a = 0$
- Oscillations are damped by the expansion of the universe
- Energy density redshifts like dark matter
- Axion stars and miniclusters

Detecting Axion Dark Matter

Axion decay to two photons:

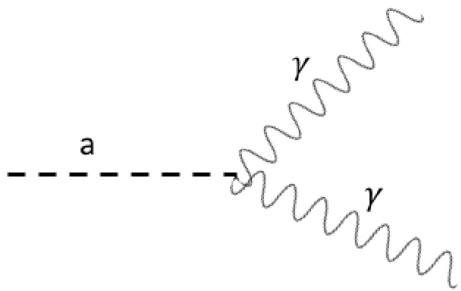

$$\Gamma_{a\to\gamma\gamma} = \frac{g_{a\gamma\gamma}^2 m_a^3}{64\pi}$$

$$E_\gamma = m_a/2$$

$$\Delta E_\gamma = E_\gamma \frac{\sigma}{c}$$

Detecting Axion Dark Matter

For $m_a \sim 1\,\mu$eV and $g_{a\gamma\gamma} \sim 10^{-10}$ GeV, $\tau \sim 10^{32}$ years. The decay rate could be significantly enhanced by stimulated decay from ambient photons. From Caputo, Regis, Taoso & Witte (1811.08436):

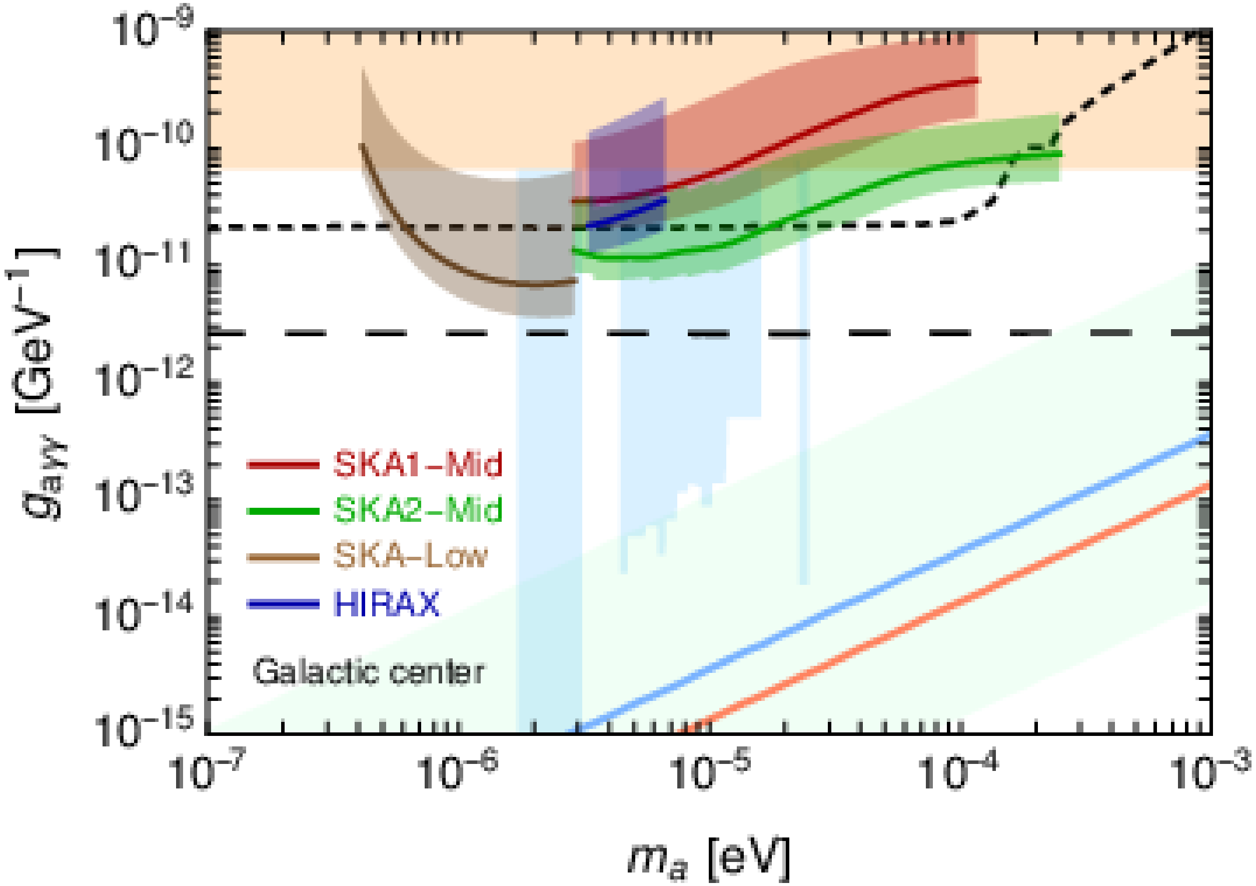

Production in stars

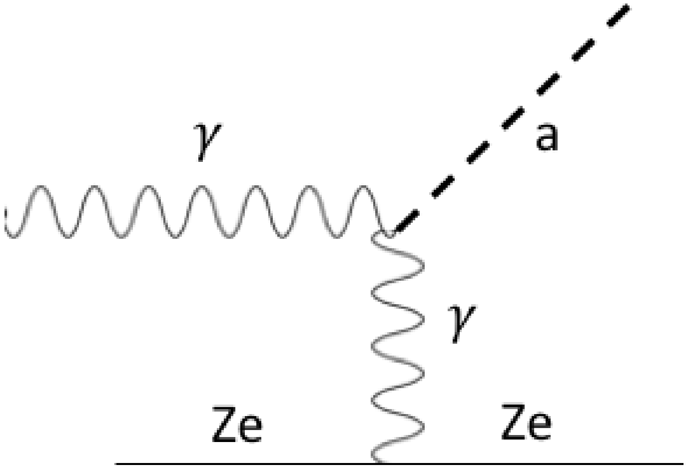

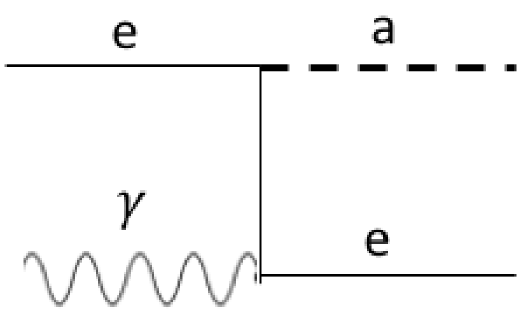

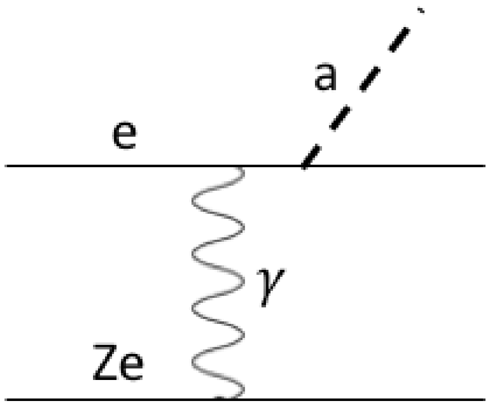

Stellar cooling from axions

- The rate of cooling depends on the stellar environment.

Stellar cooling from axions

- The rate of cooling depends on the stellar environment.
- Therefore we can place bounds on axions using the number of stars observed in each stellar phase. (Raffelt & Dearborn 1987)

Stellar cooling from axions

- The rate of cooling depends on the stellar environment.
- Therefore we can place bounds on axions using the number of stars observed in each stellar phase. (Raffelt & Dearborn 1987)
- Bounds on $g_{a\gamma\gamma}$ from ratio of Red Giant Branch to Horizontal Branch stars. (Ayala *et al*, 1406.6053)

Stellar cooling from axions

- The rate of cooling depends on the stellar environment.
- Therefore we can place bounds on axions using the number of stars observed in each stellar phase. (Raffelt & Dearborn 1987)
- Bounds on $g_{a\gamma\gamma}$ from ratio of Red Giant Branch to Horizontal Branch stars. (Ayala *et al*, 1406.6053)
- Bounds on g_{aee} from the brightness of the Red Giant Branch (Viaux *et al*, 1311.1669), and from the luminosity function of white dwarfs (Raffelt 1986 and Blinnikov & Dunina-Barkovskaya, 1994).

Stellar cooling from axions

- The rate of cooling depends on the stellar environment.
- Therefore we can place bounds on axions using the number of stars observed in each stellar phase. (Raffelt & Dearborn 1987)
- Bounds on $g_{a\gamma\gamma}$ from ratio of Red Giant Branch to Horizontal Branch stars. (Ayala *et al*, 1406.6053)
- Bounds on g_{aee} from the brightness of the Red Giant Branch (Viaux *et al*, 1311.1669), and from the luminosity function of white dwarfs (Raffelt 1986 and Blinnikov & Dunina-Barkovskaya, 1994).
- This method constrains $g_{aee} < 9 \times 10^{-10}\,\mathrm{GeV}^{-1}$

Stellar cooling from axions

- The rate of cooling depends on the stellar environment.
- Therefore we can place bounds on axions using the number of stars observed in each stellar phase. (Raffelt & Dearborn 1987)
- Bounds on $g_{a\gamma\gamma}$ from ratio of Red Giant Branch to Horizontal Branch stars. (Ayala *et al*, 1406.6053)
- Bounds on g_{aee} from the brightness of the Red Giant Branch (Viaux *et al*, 1311.1669), and from the luminosity function of white dwarfs (Raffelt 1986 and Blinnikov & Dunina-Barkovskaya, 1994).
- This method constrains $g_{aee} < 9 \times 10^{-10}\,\mathrm{GeV}^{-1}$
- Axion hints from stellar cooling?

Stellar cooling limits

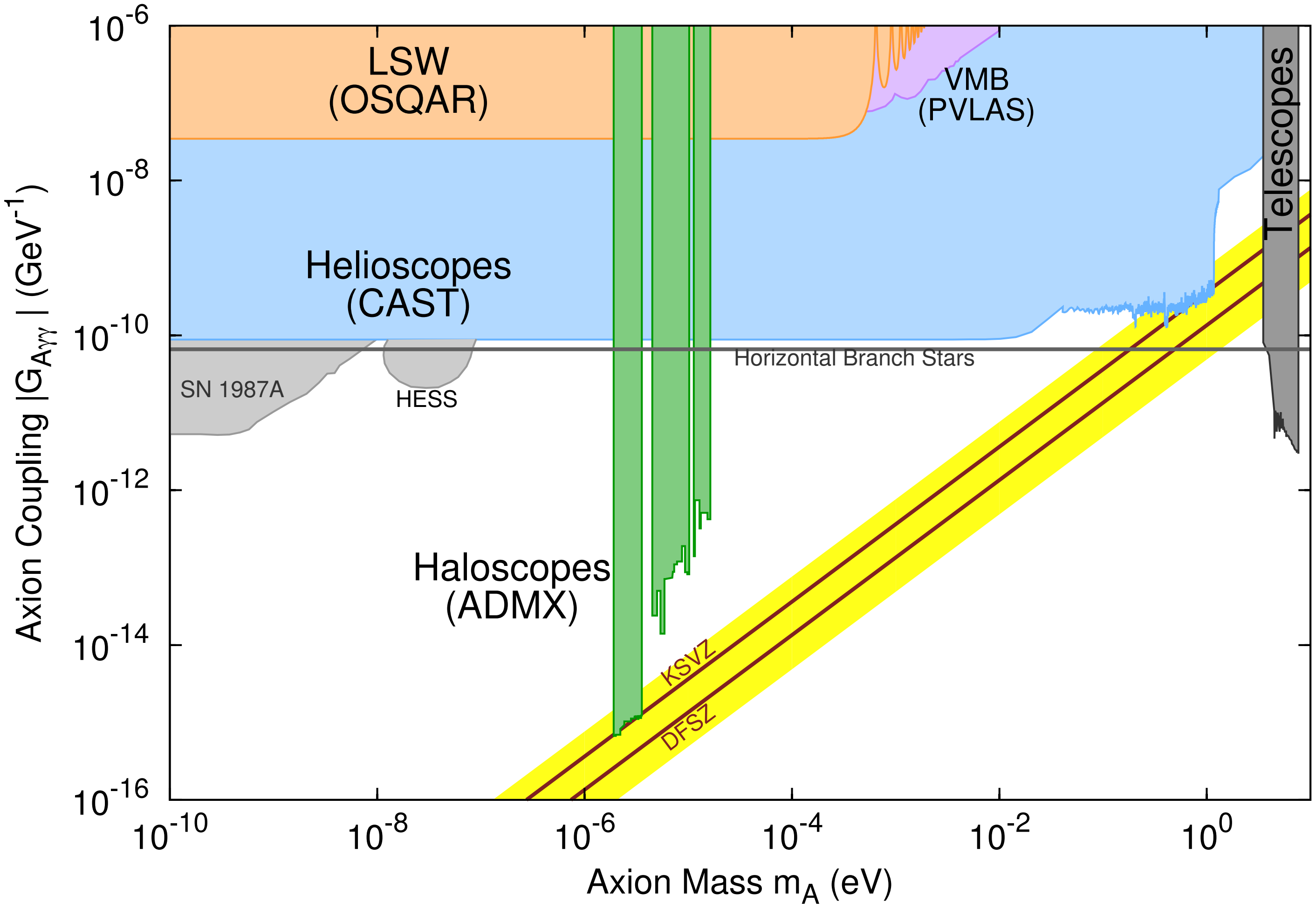

Reproduced from the Particle Data Group

SN bound: Brockway, Carlson & Raffelt, astro-ph/9605197

Black Hole Superradiance

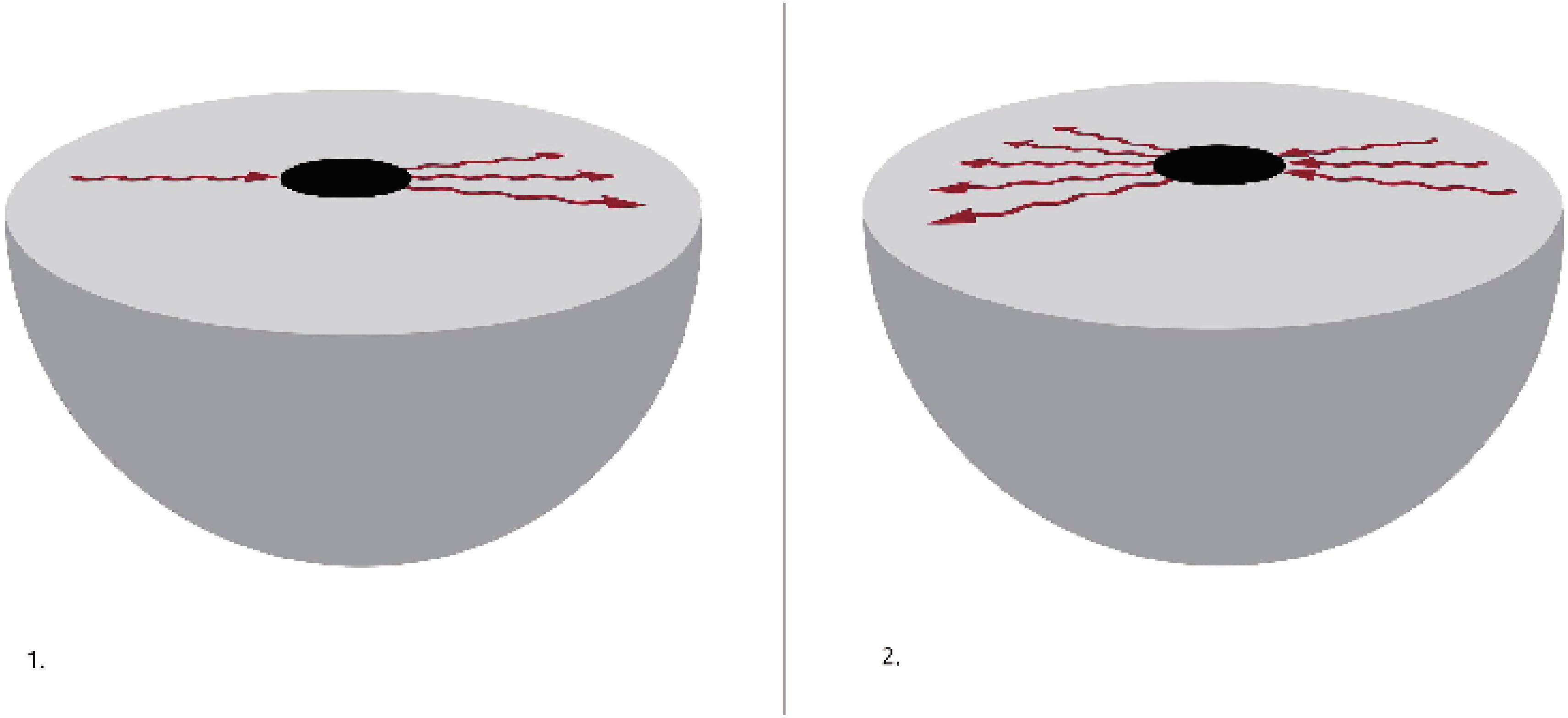

Reproduced from Brito, Cardosa & Pani, 1501.06570

Axion Black Hole Superradiance

- Axions build up around Kerr black hole

Axion Black Hole Superradiance

- Axions build up around Kerr black hole
- 'Bosenova' explosion as axion cloud collapses (Arvanitaki & Dubovsky, 1004.3558)

Axion Black Hole Superradiance

- Axions build up around Kerr black hole
- 'Bosenova' explosion as axion cloud collapses (Arvanitaki & Dubovsky, 1004.3558)
- Depletion of black hole spin

Axion Black Hole Superradiance

- Axions build up around Kerr black hole
- 'Bosenova' explosion as axion cloud collapses (Arvanitaki & Dubovsky, 1004.3558)
- Depletion of black hole spin
- Stellar mass BH spin measurements exclude $6 \times 10^{-13}\,\mathrm{eV} < m_a < 2 \times 10^{-11}\,\mathrm{eV}$ for $f_a \gtrsim 10^{13}\,GeV$. (Arvanitaki, Baryakhtar & Huang, 1411.2263)

Axion Black Hole Superradiance

- Axions build up around Kerr black hole
- 'Bosenova' explosion as axion cloud collapses (Arvanitaki & Dubovsky, 1004.3558)
- Depletion of black hole spin
- Stellar mass BH spin measurements exclude $6 \times 10^{-13}\,\mathrm{eV} < m_a < 2 \times 10^{-11}\,\mathrm{eV}$ for $f_a \gtrsim 10^{13} GeV$. (Arvanitaki, Baryakhtar & Huang, 1411.2263)
- Advanced Ligo will be sensitive to $m_a \lesssim 10^{-10}\,\mathrm{eV}$. (Arvanitaki *et al*, 1604.03958).

Axion Black Hole Superradiance

- Axions build up around Kerr black hole
- 'Bosenova' explosion as axion cloud collapses (Arvanitaki & Dubovsky, 1004.3558)
- Depletion of black hole spin
- Stellar mass BH spin measurements exclude $6 \times 10^{-13}\,\mathrm{eV} < m_a < 2 \times 10^{-11}\,\mathrm{eV}$ for $f_a \gtrsim 10^{13}\,GeV$. (Arvanitaki, Baryakhtar & Huang, 1411.2263)
- Advanced Ligo will be sensitive to $m_a \lesssim 10^{-10}\,\mathrm{eV}$. (Arvanitaki *et al*, 1604.03958).
- Constraints on the axiverse mass spectrum (Stott & Marsh, 1805.02016)

Axion-photon conversion

$$\left(\omega + \begin{pmatrix} \Delta_\gamma & 0 & \Delta_{\gamma a x} \\ 0 & \Delta_\gamma & \Delta_{\gamma a y} \\ \Delta_{\gamma a x} & \Delta_{\gamma a y} & \Delta_a \end{pmatrix} - i\partial_z\right)\begin{pmatrix} |\,\gamma_x\rangle \\ |\,\gamma_y\rangle \\ |\,a\rangle \end{pmatrix} = 0$$

- $\Delta_\gamma = \frac{-\omega_{pl}^2}{2\omega}$
- Plasma frequency: $\omega_{pl} = \left(4\pi\alpha\frac{n_e}{m_e}\right)^{\frac{1}{2}}$
- $\Delta_a = \frac{-m_a^2}{\omega}$.
- Here we take $m_a = 0$. This is valid for $m_a \lesssim 10^{-12}\,\mathrm{eV}$.
- Mixing: $\Delta_{\gamma a i} = \frac{B_i}{2M}$

$$P_{a\to\gamma}(L) = |\,\langle 1,0,0|f(L)\rangle\,|^2 + |\,\langle 0,1,0|f(L)\rangle\,|^2$$

Anomalous Transparency Hint

- Axions and photons can interconvert in the magnetic fields of galaixes, galaxy clusters, AGN, intergalactic space ...

Anomalous Transparency Hint

- Axions and photons can interconvert in the magnetic fields of galaixes, galaxy clusters, AGN, intergalactic space ...
- Photons above ~ 100 GeV are attenuated in intergalactic space due to pair production with extra-galactic background light.

Anomalous Transparency Hint

- Axions and photons can interconvert in the magnetic fields of galaixes, galaxy clusters, AGN, intergalactic space ...
- Photons above ~ 100 GeV are attenuated in intergalactic space due to pair production with extra-galactic background light.
- The universe might be more transparent to such very high energy photons than we thought (Horns & Meyer 1201.4711).

Anomalous Transparency Hint

- Axions and photons can interconvert in the magnetic fields of galaixes, galaxy clusters, AGN, intergalactic space ...
- Photons above ~ 100 GeV are attenuated in intergalactic space due to pair production with extra-galactic background light.
- The universe might be more transparent to such very high energy photons than we thought (Horns & Meyer 1201.4711).
- This anomaly can be explained by interconversion with axions, as an intergalactic example of light shining through a wall.

Anomalous Transparency Hint

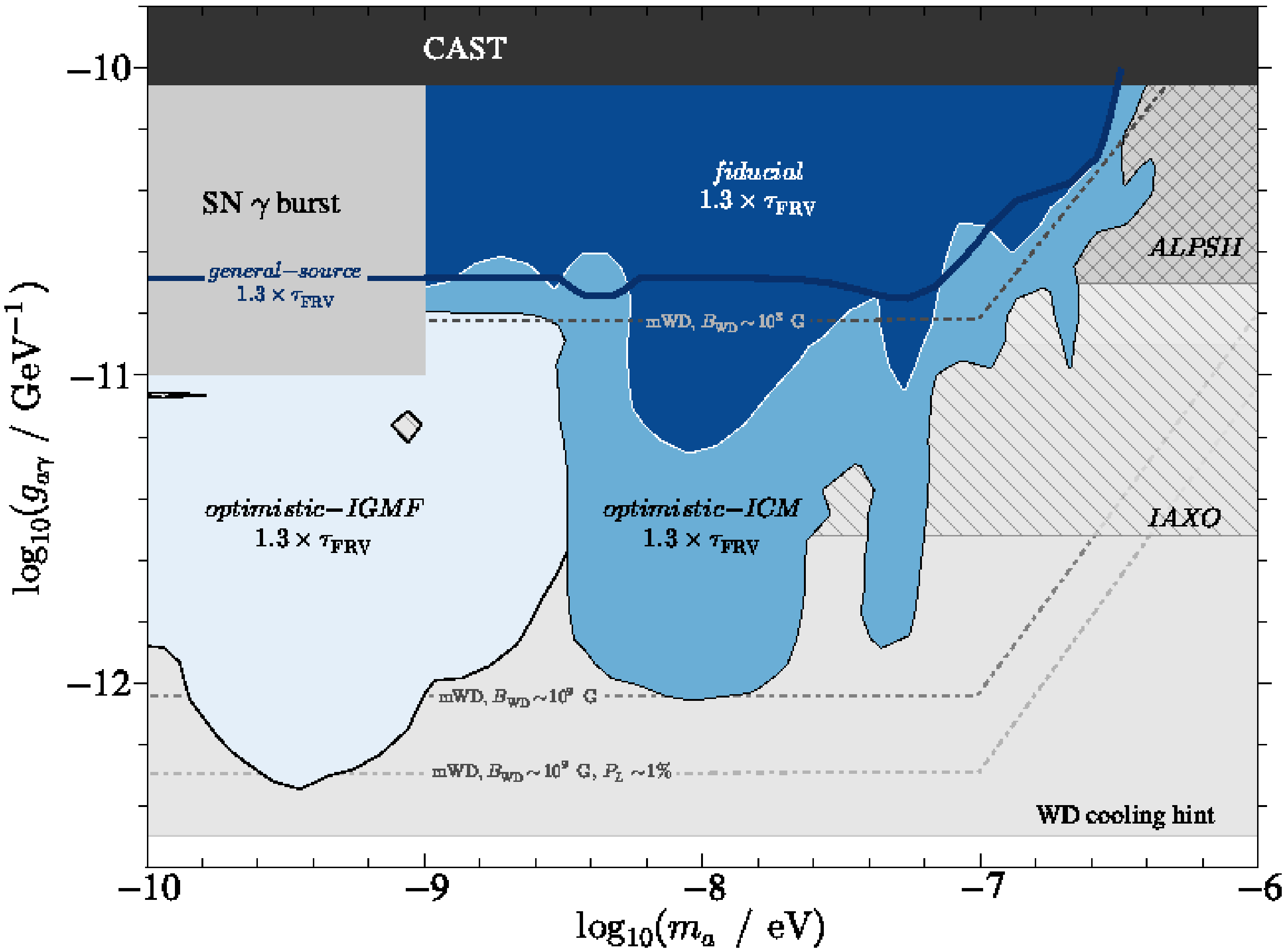

Reproduced from Meyer, Horns & Raue, 1302.1208.

Galaxy clusters

Photon survival probability

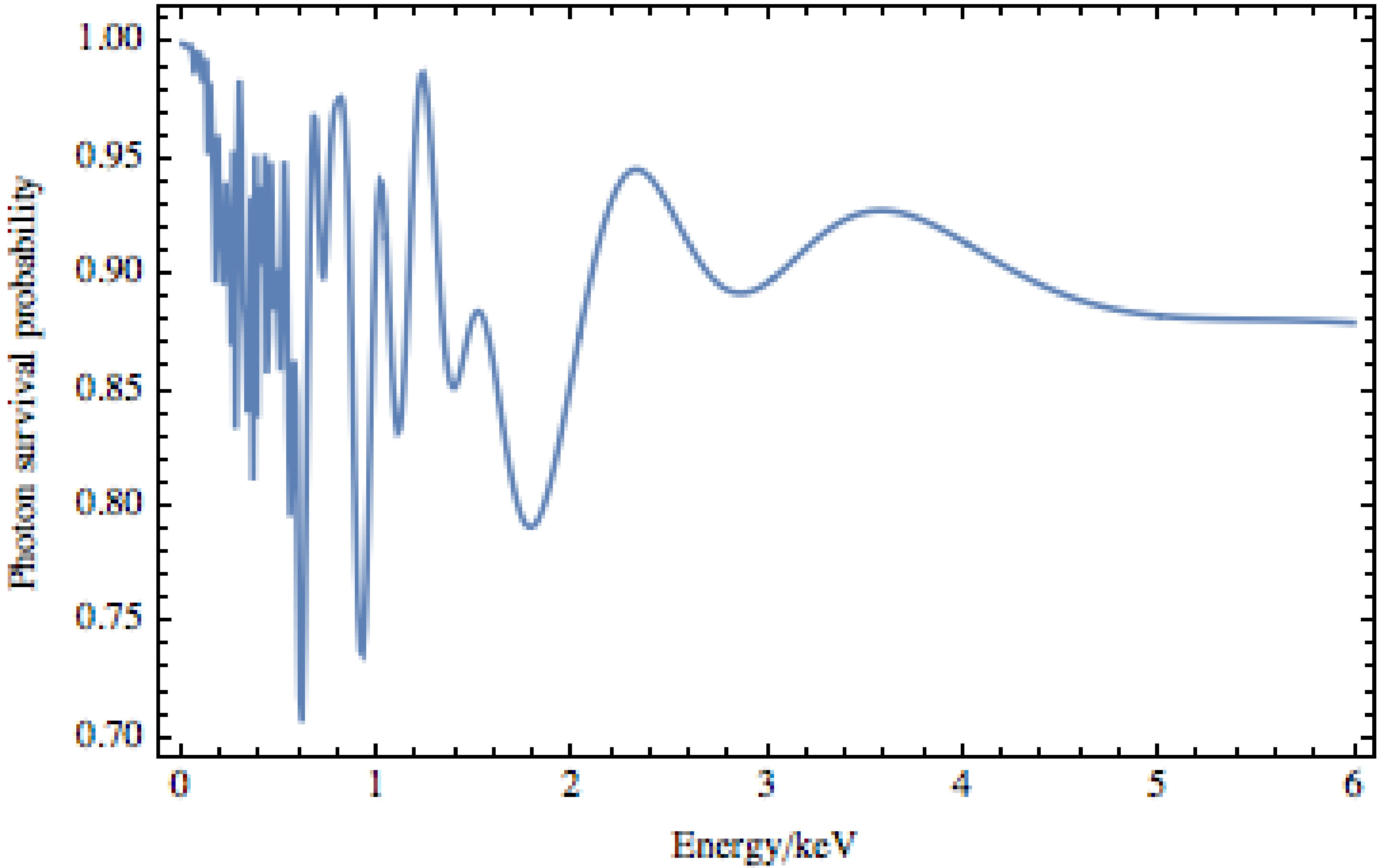

Bounds

The leading bounds are from NGC1275 in Perseus, 2E3140 in A1795 and M87 in Virgo: $M \gtrsim 7 \times 10^{11}$ GeV.

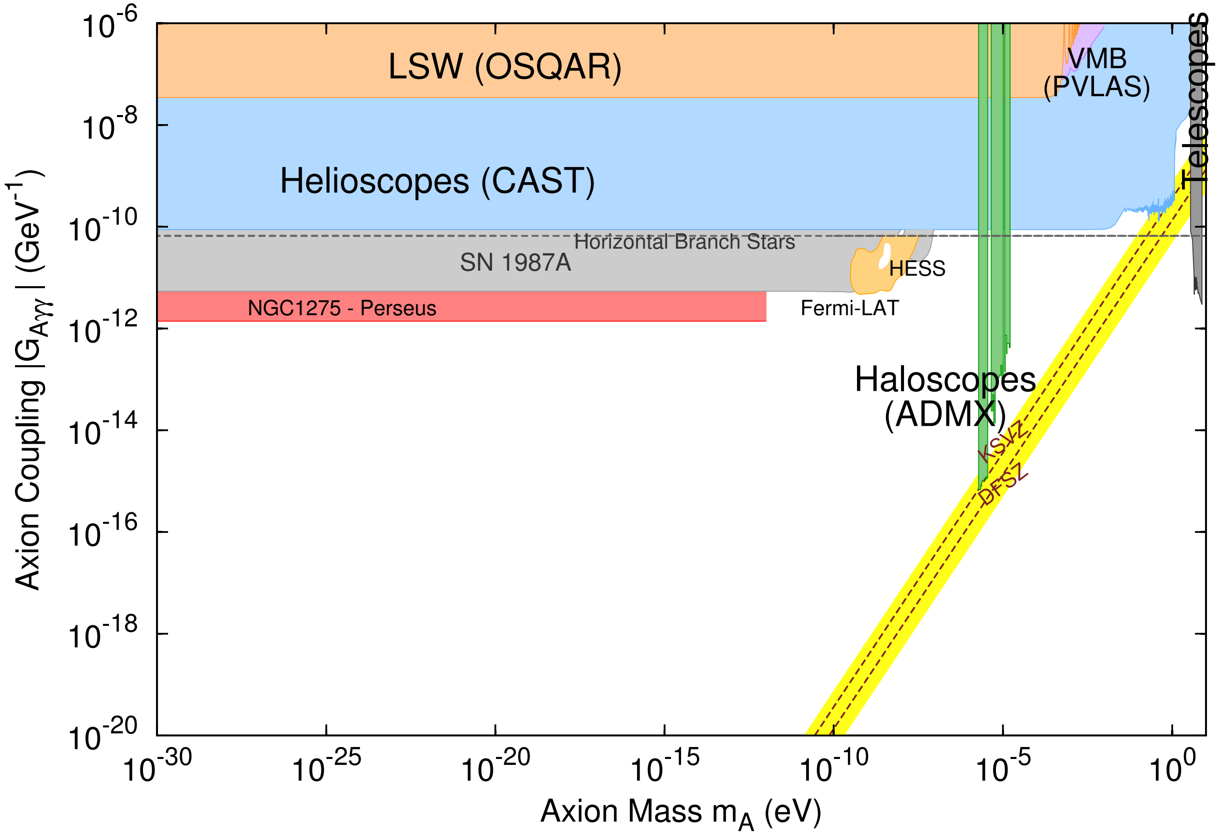

Fermi-LAT Collaboration (1603.06978), M Berg *et al* (1605.01043), J Conlon *et al* (1704.05256), D Marsh *et al* (1703.07354)

Axion-photon conversion

$$\left(\omega + \begin{pmatrix} \Delta_\gamma & 0 & \Delta_{\gamma ax} \\ 0 & \Delta_\gamma & \Delta_{\gamma ay} \\ \Delta_{\gamma ax} & \Delta_{\gamma ay} & \Delta_a \end{pmatrix} - i\partial_z\right) \begin{pmatrix} |\gamma_x\rangle \\ |\gamma_y\rangle \\ |a\rangle \end{pmatrix} = 0$$

Only the photon polarization parallel to the external magnetic field participates in axion-photon conversion.

IXPE

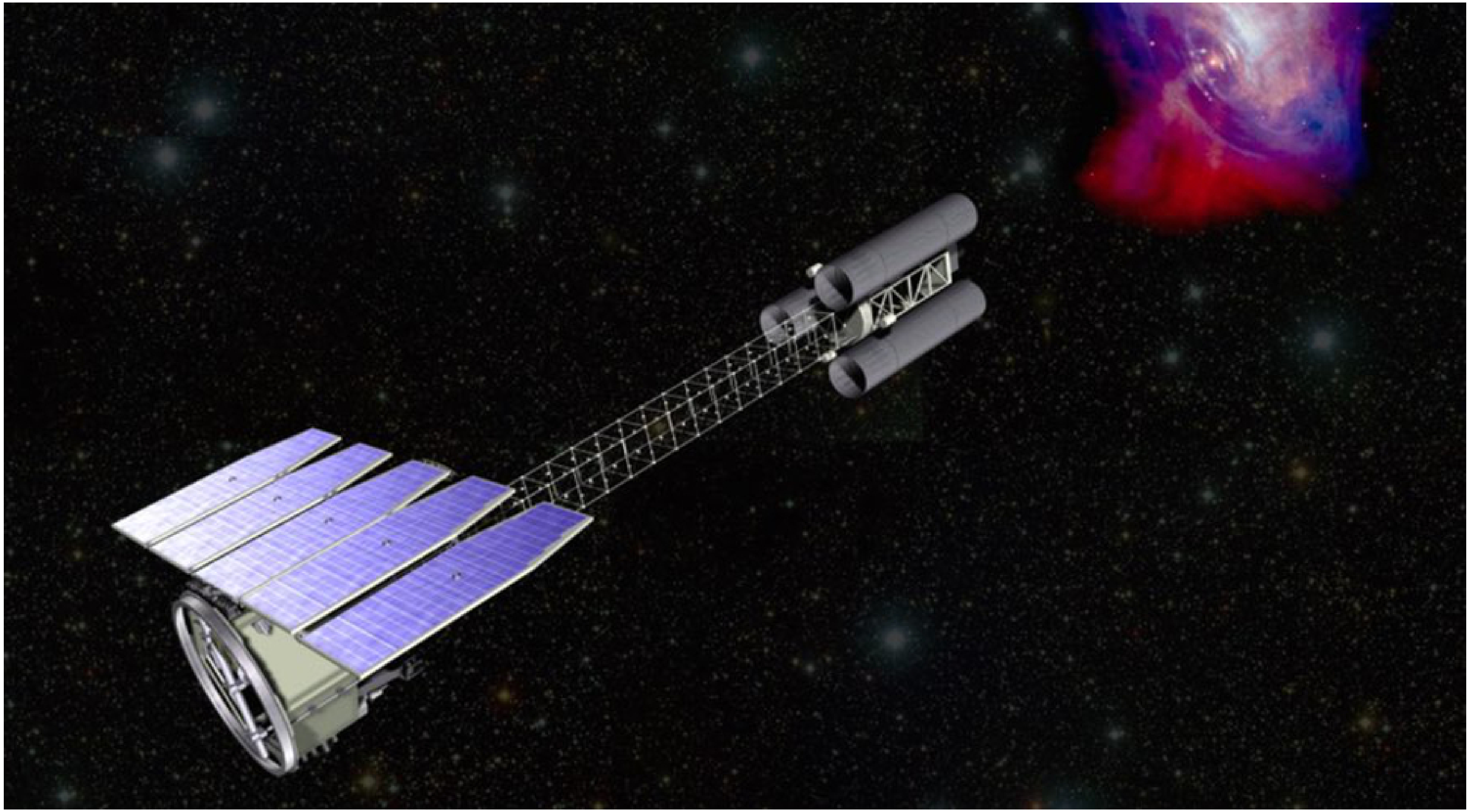

Polarimetry oscillations

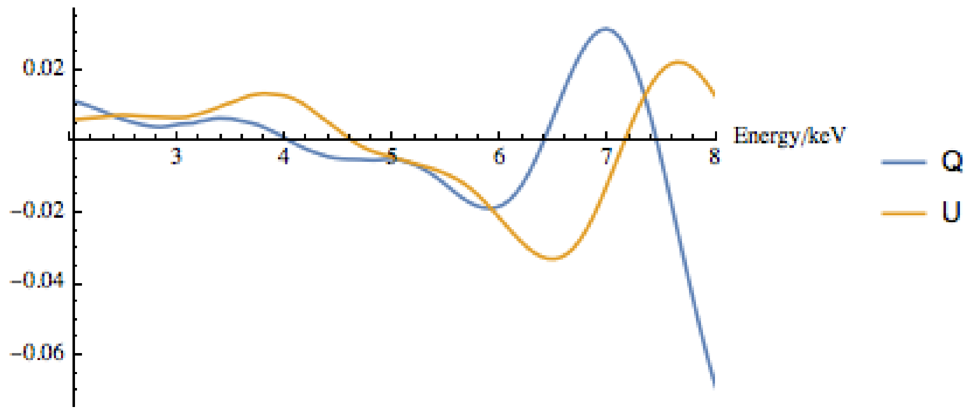

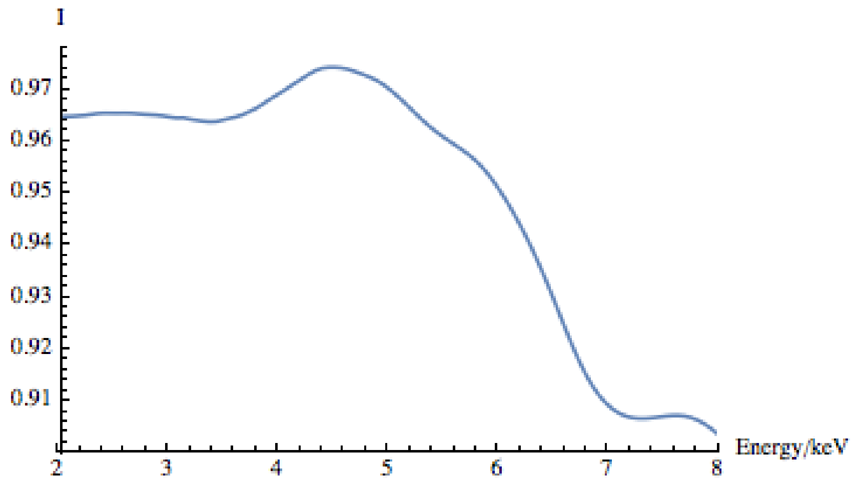

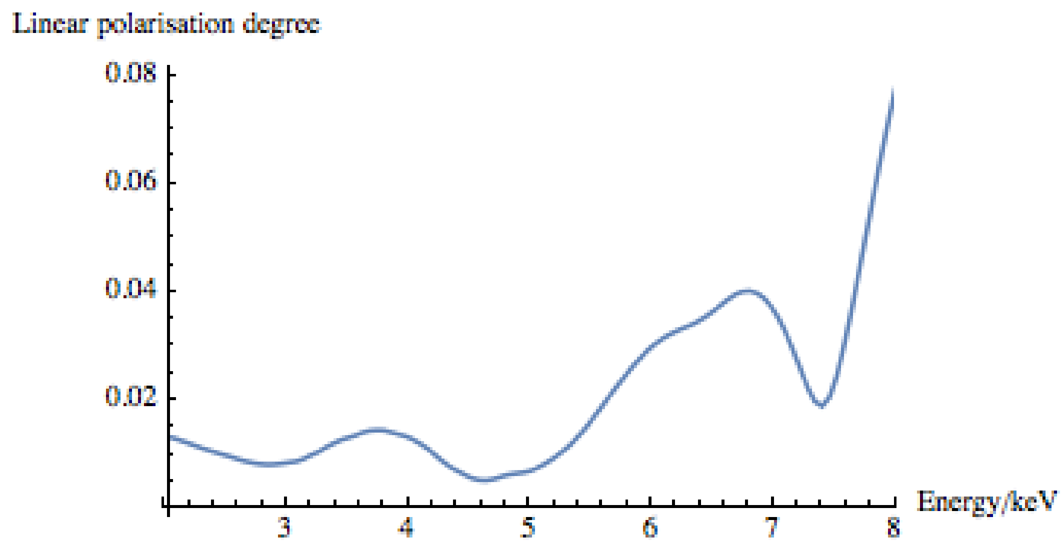

Polarimetry bounds

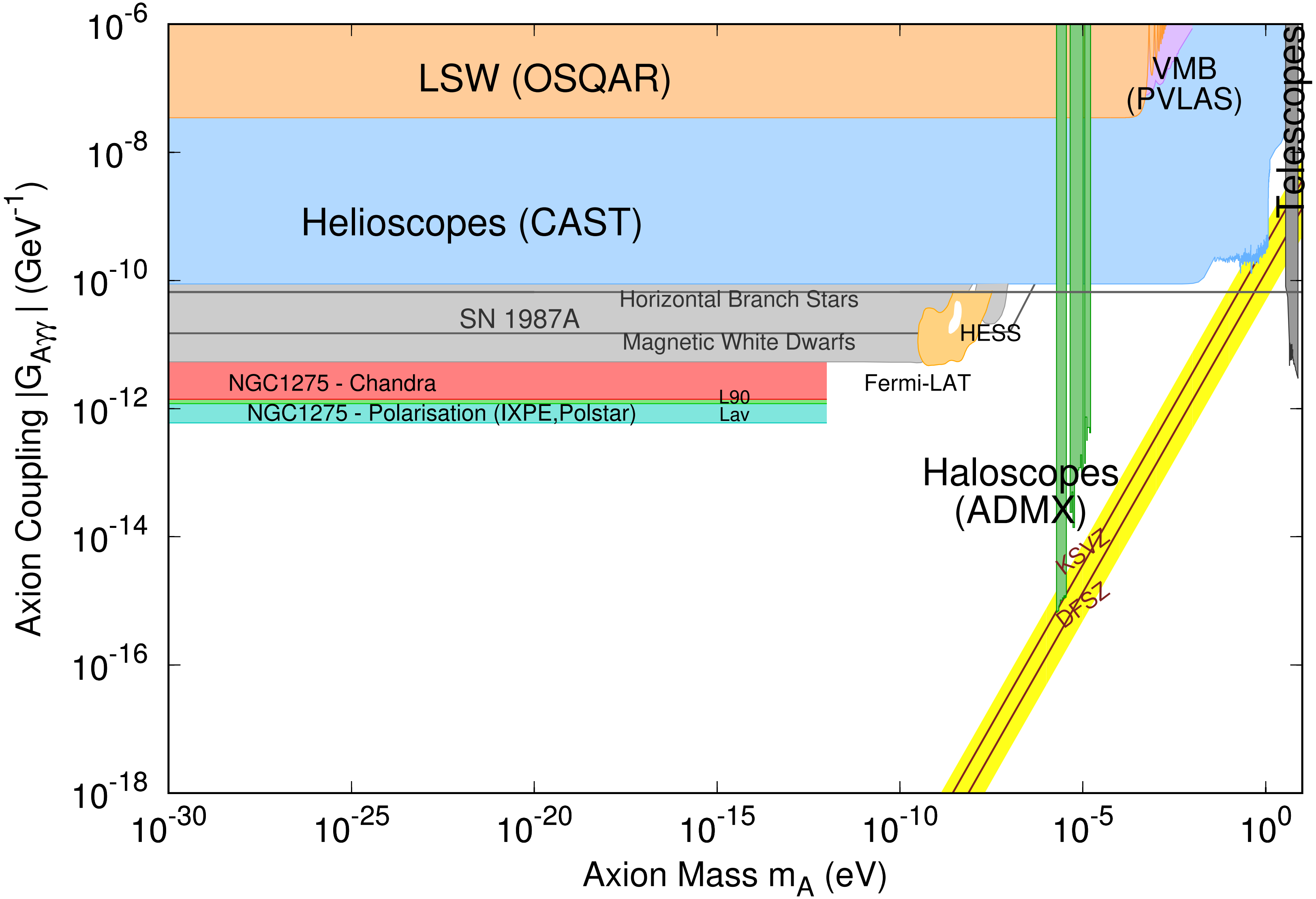

(Day & Krippendorf, 1801.10557)

Conclusions

- Astrophysical environments are excellent places to search for axions.
- The next generation of telescopes, as well as gravitational wave astronomy, will allow us to place even more stringent bounds on axions.
- Photons, neutrinos and gravitational waves all play key roles in axion searches.

Single domain

$$
\begin{aligned}
\tan(2\theta) &= 10.0 \times 10^{-3} \times \left(\frac{10^{-3}\,\mathrm{cm}^{-3}}{n_e}\right)\left(\frac{B_\perp}{1\,\mu\mathrm{G}}\right)\left(\frac{\omega}{3.5\,\mathrm{keV}}\right)\left(\frac{10^{13}\,\mathrm{GeV}}{M}\right) \\
\Delta &= 0.015 \times \left(\frac{n_e}{10^{-3}\,\mathrm{cm}^{-3}}\right)\left(\frac{3.5\,\mathrm{keV}}{\omega}\right)\left(\frac{L}{1\,\mathrm{kpc}}\right)
\end{aligned}
$$

$$
P(a \rightarrow \gamma) = \sin^2(2\theta)\sin^2\left(\frac{\Delta}{\cos 2\theta}\right)
$$

Small angle approximation

Over a distance R of $R/L \gg 1$ domains, with **B** randomised between each domain, we can approximate:

$$P \simeq 6.9 \times 10^{-7} \left(\frac{L}{1\,\mathrm{kpc}} \frac{R}{30\,\mathrm{kpc}} \right) \left(\frac{B_\perp}{1\,\mu\mathrm{G}} \frac{10^{13}\,\mathrm{GeV}}{M} \right)^2$$

for $\theta, \Delta \ll 1$

In most astrophysical environments with have $\theta \ll 1$ but not always $\Delta \ll 1$.

Axion-photon conversion

- $P_{a\to\gamma} \propto \frac{B_\perp^2}{M^2}$ for $\frac{B_\perp^2}{M^2} \ll 1$
- $P_{a\to\gamma}$ increases with the field coherence length and the total extent of the field.
- High electron densities increase the effective photon mass, suppressing conversion.
- Astrophysical environments lead to the highest conversion probabilities.
- The conversion probability is pseudo-sinusoidal in $1/E$.
- Hints from galaxy cluster soft X-ray excess and 3.5 keV line.

Semi-analytic formula

For $P_{a\to\gamma} \ll 1$:

$$P_{a\to\gamma}(L) = \sum_{i=x,y} \left| \int_0^L dz e^{i\varphi(z)} \Delta_{\gamma a i}(z) \right|^2 , \qquad (1)$$

where,

$$\varphi(z) = \int_0^z dz' \Delta_\gamma(z') = -\frac{1}{\omega} \int_0^z dz' \omega_{pl}^2(z') . \qquad (2)$$

- $\Delta_\gamma(z) \propto n_e$
- Electron density rotates the probability amplitudes $\langle 1,0,0|f(L)\rangle$ and $\langle 0,1,0|f(L)\rangle$ in the complex plane as L increases, suppressing the efficacy of the magnetic field in increasing the conversion probability over increasing distances.

Photoelectric absorption

Use density matrix formalism to include photo-electric absorption of photon components:
Damping parameter: $\Gamma = \sigma_{\rm eff}\left(n_{HI} + 2n_{H2}\right)$

$$H = \begin{pmatrix} \Delta_\gamma & 0 & \Delta_{\gamma ax} \\ 0 & \Delta_\gamma & \Delta_{\gamma ay} \\ \Delta_{\gamma ax} & \Delta_{\gamma ay} & \Delta_a \end{pmatrix} - \begin{pmatrix} i\frac{\Gamma}{2} & 0 & 0 \\ 0 & i\frac{\Gamma}{2} & 0 \\ 0 & 0 & 0 \end{pmatrix} = M - iD,$$

$$\rho = \begin{pmatrix} \mid \gamma_x \rangle \\ \mid \gamma_y \rangle \\ \mid a \rangle \end{pmatrix} \otimes \begin{pmatrix} \mid \gamma_x \rangle & \mid \gamma_y \rangle & \mid a \rangle \end{pmatrix}^*$$

$$\rho(z) = e^{-iHz}\rho(0)e^{iH^\dagger z}.$$

Analysis

We analyse 8 likely looking point sources:

- The AGN NGC1275 at the centre of Perseus
- The quasars B1256+281 and SDSS J130001.48+275120.6 shining through Coma
- The AGN NGC3862 in A1367
- The AGN IC4374 at the centre of A3581
- The bright Sy1 galaxy 2E3140 within A1795
- The quasar CXOU J134905.8+263752 behind A1795
- The central AGN UGC9799 of the cluster A2052

Example: NGC3862 in A1367

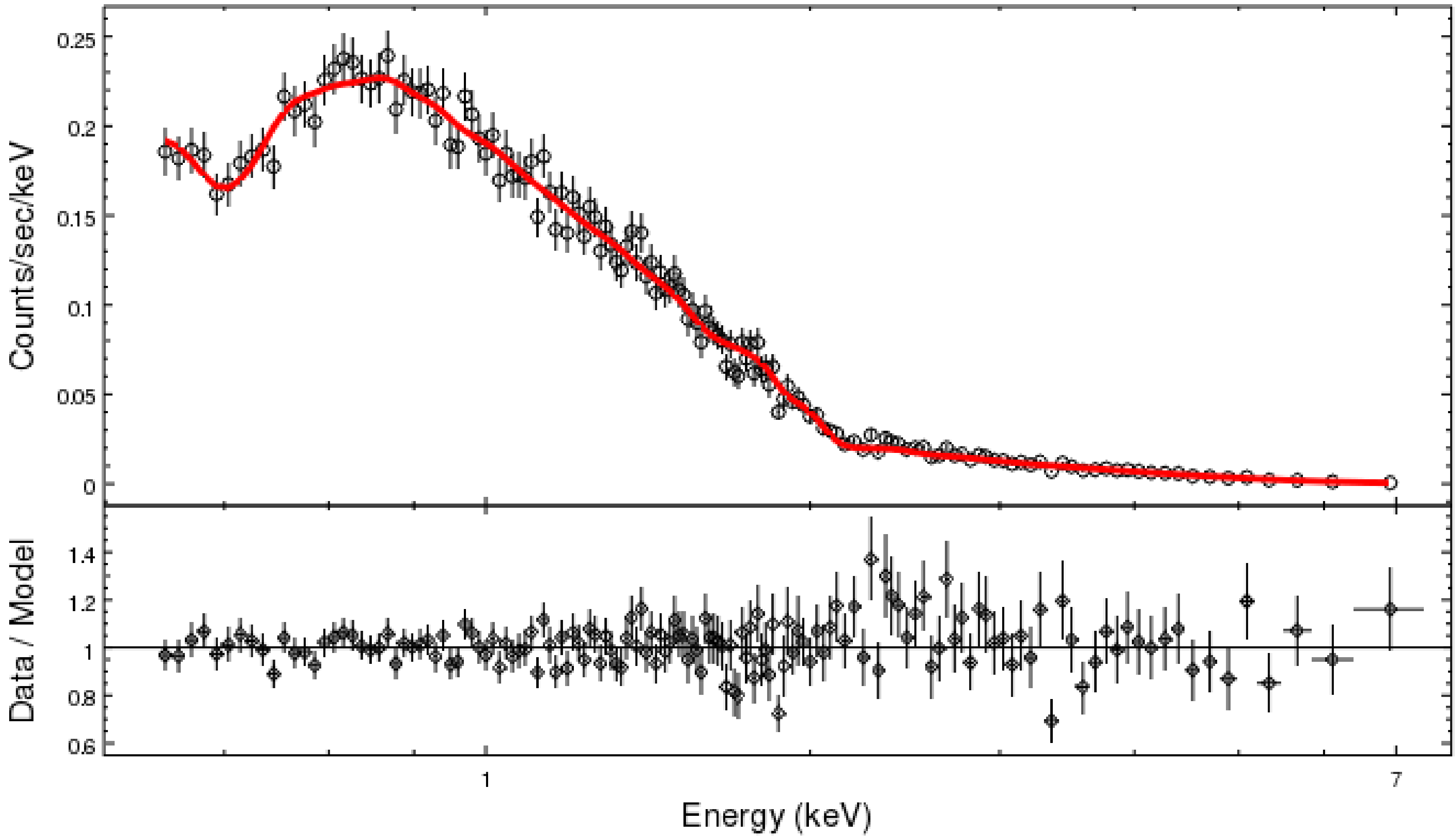

Projected bounds with Athena

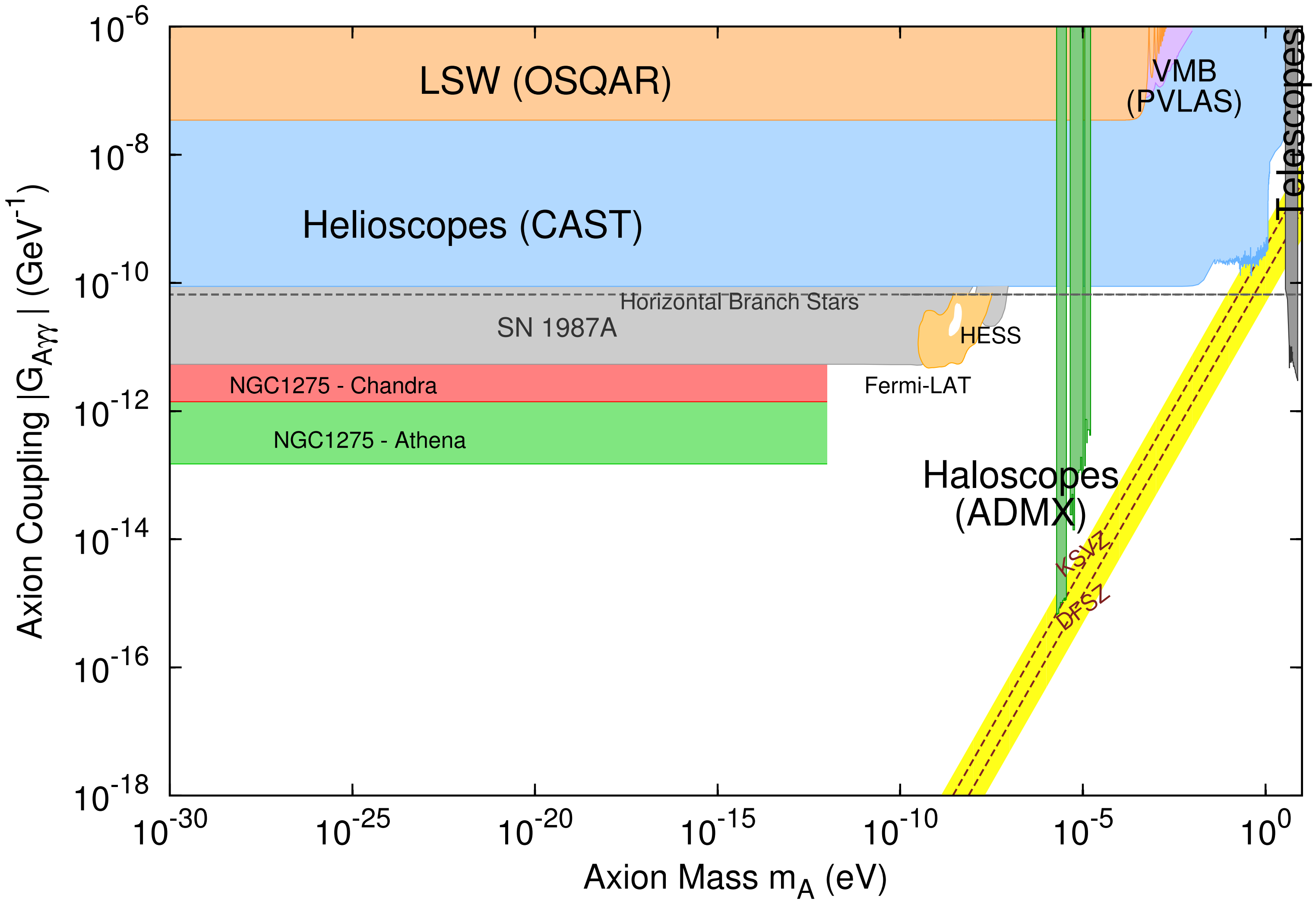

J Conlon *et al*, (1707.00176)

Stokes parameters

$$I = E_x^2 + E_y^2$$

$$Q = E_x^2 - E_y^2$$

$$U = 2\mathcal{R}e\left(E_x E_y^*\right)$$

$$V = -2\mathcal{I}m\left(E_x E_y^*\right)$$

$$p_{\rm lin} = \frac{\sqrt{Q^2+U^2}}{I}$$

$$\psi = \frac{1}{2}\tan^{-1}\left(\frac{U}{Q}\right)$$

Measurement

Basic implementation of detector errors from Kislat *et al* (1409.6214), using measured flux from NGC1275 and background from Perseus:

$$P(p_{\rm lin}, \psi | p_0, \psi_0) = \frac{\sqrt{I^2/W_2}\, p_{\rm lin}\mu^2}{2\pi\sigma} \times$$

$$\exp\left[-\frac{\mu^2}{4\sigma^2}\{p_0^2 + p_{\rm lin}^2 - 2p_0 p_{\rm lin}\cos(2(\psi_0 - \psi)) - \frac{p_0^2 p_{\rm lin}^2 \mu^2}{2}\sin^2(2(\psi - \psi_0))\}\right]$$

With

$$W_2 = (R_S + R_{BG})T(1 - f_{\rm off}) + R_{BG}Tf_{\rm off}\left(\frac{1 - f_{\rm off}}{f_{\rm off}}\right)^2, \tag{4}$$

And

$$\sigma = \sqrt{\frac{W_2}{I^2}\left(1 - \frac{p_0^2\mu^2}{2}\right)}. \tag{5}$$

Polarimetry bounds

- Initially assume a featureless intrinsic AGN polarisation of 0%, 1% or 5%.
- Use the magnetic field experienced by photons from NGC1275 travelling through Perseus, marginalising over different field configurations
- Bin to IXPE's energy resolution
- Compare a constant polarisation hypothesis with a constant source polarisation altered by axions

Next Steps

- Realistic source polarisation spectra
- Instrumental modelling

AGN

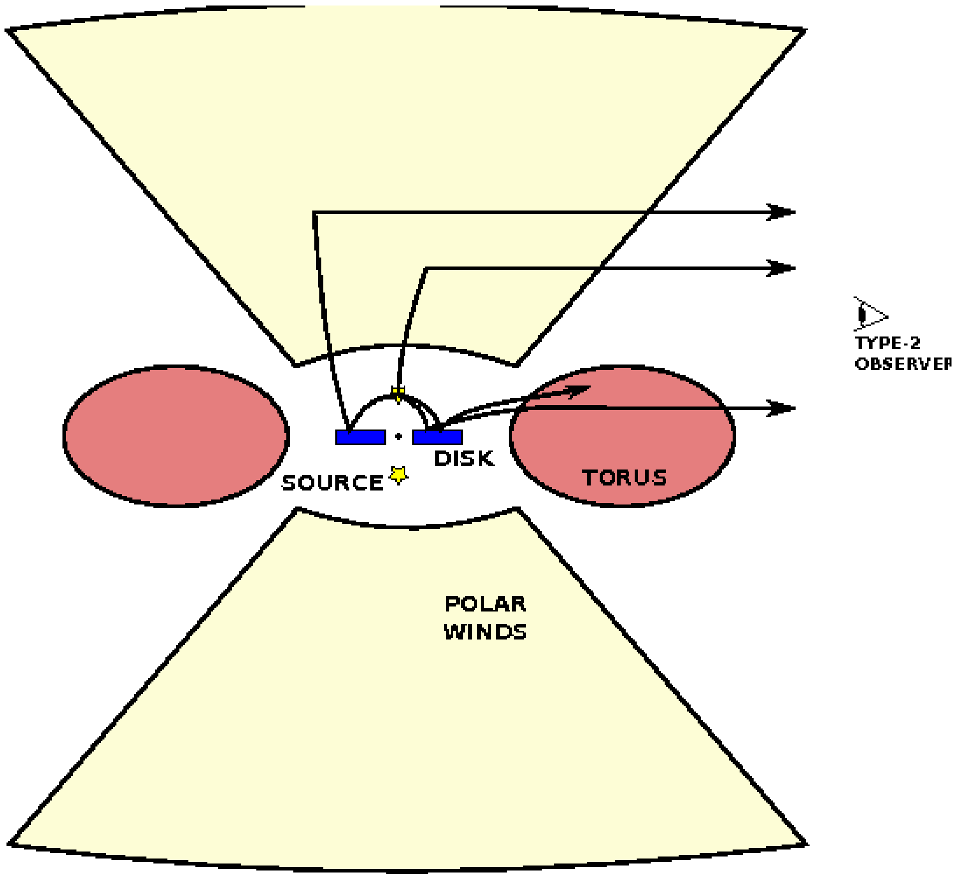

Reproduced from F Marin *et al*, 1709.03304

Type I AGN polarization

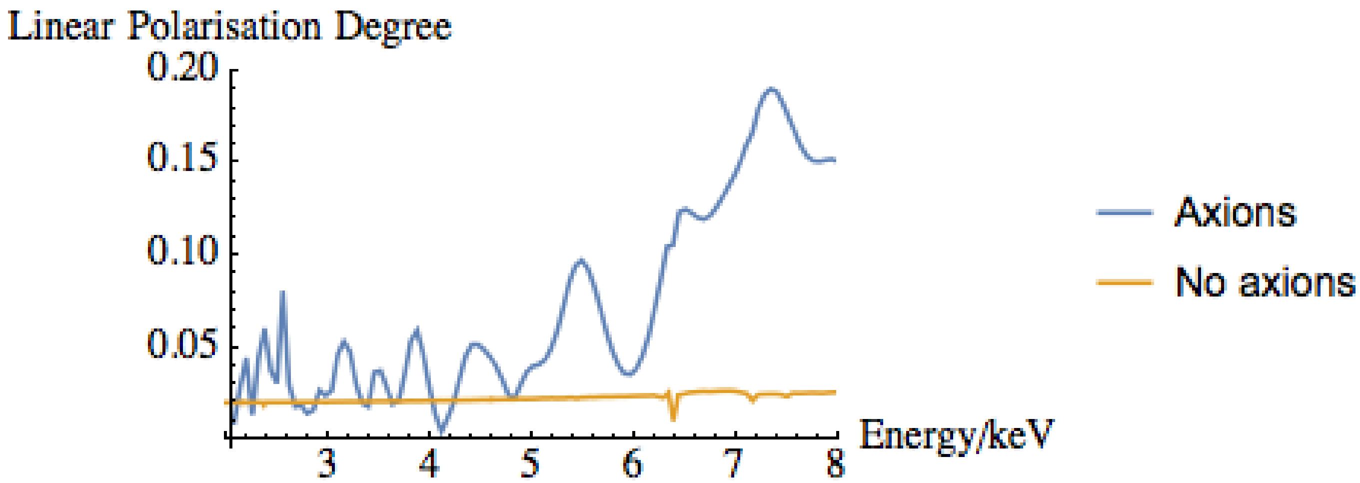

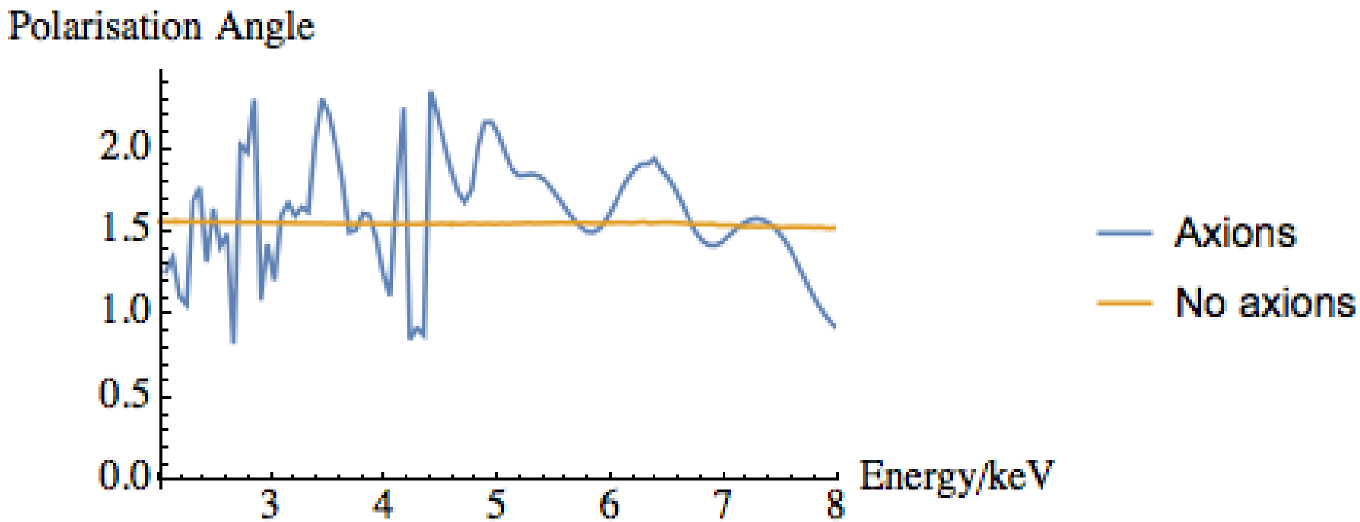

$g_{a\gamma\gamma} = 10^{-12}\,\mathrm{GeV}^{-1}$

Type I AGN polarization

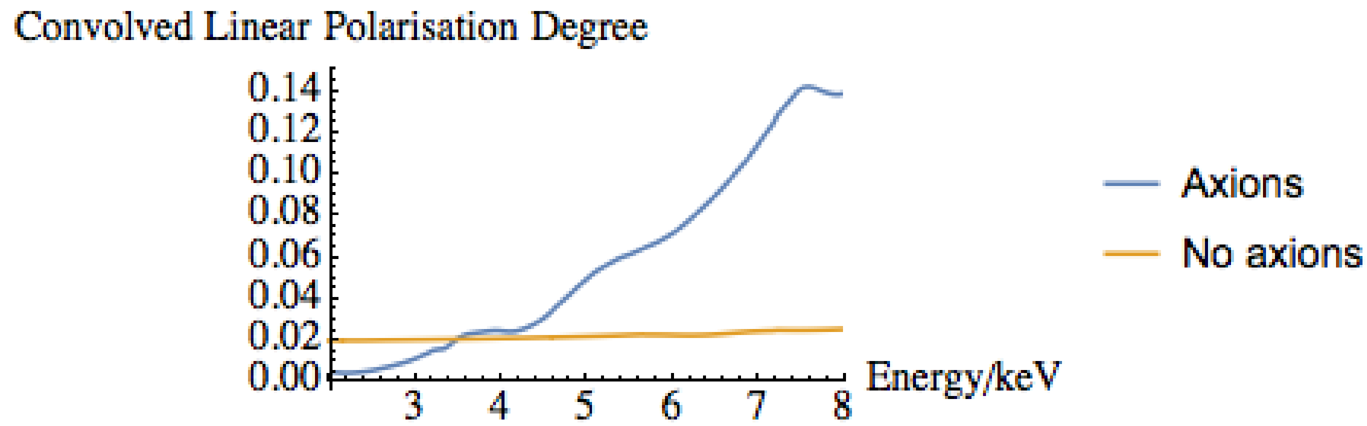

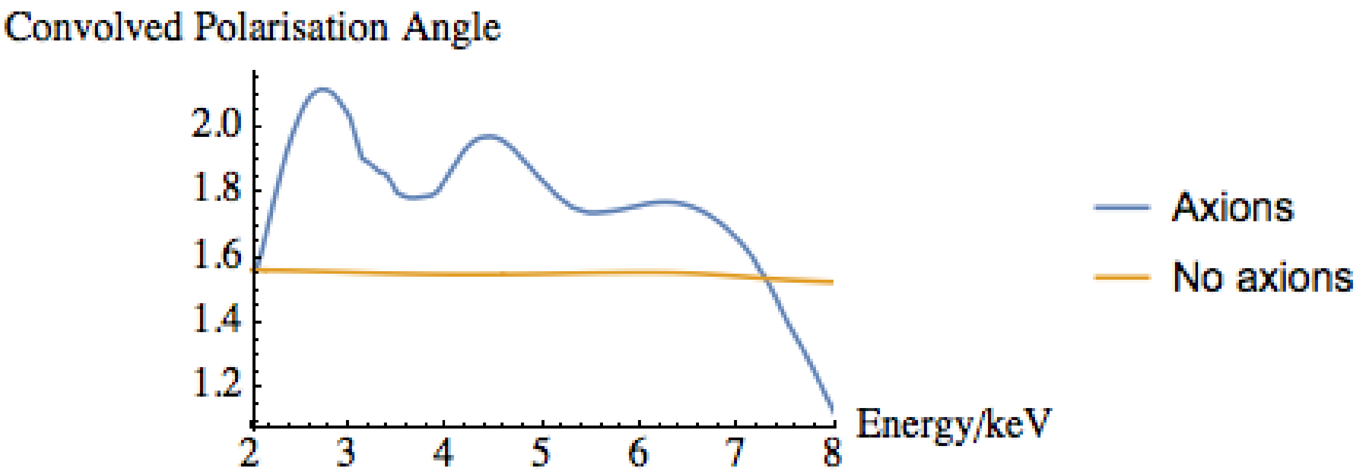

$$g_{a\gamma\gamma} = 10^{-12}\,\mathrm{GeV}^{-1}$$

Type I AGN polarization

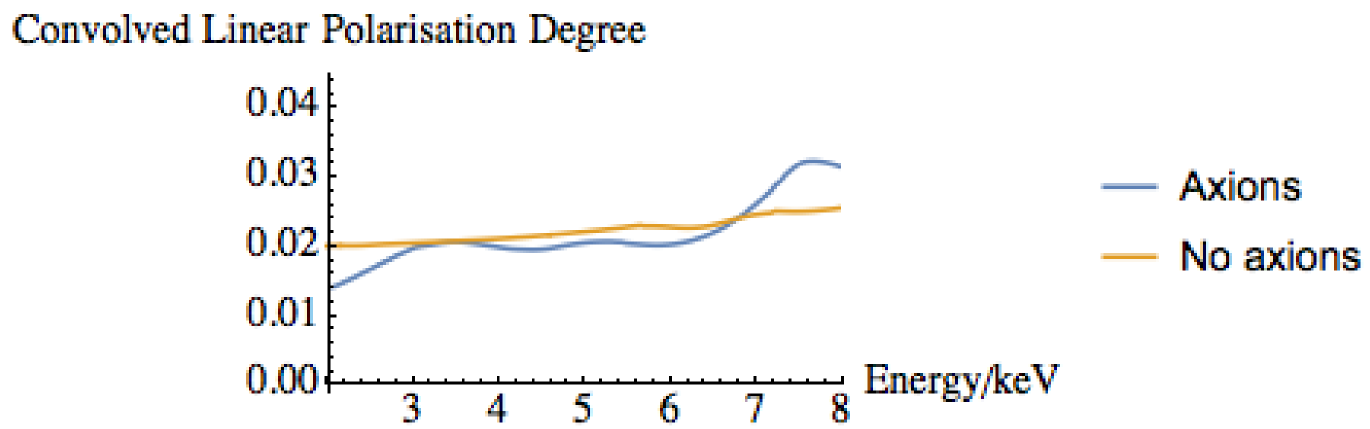

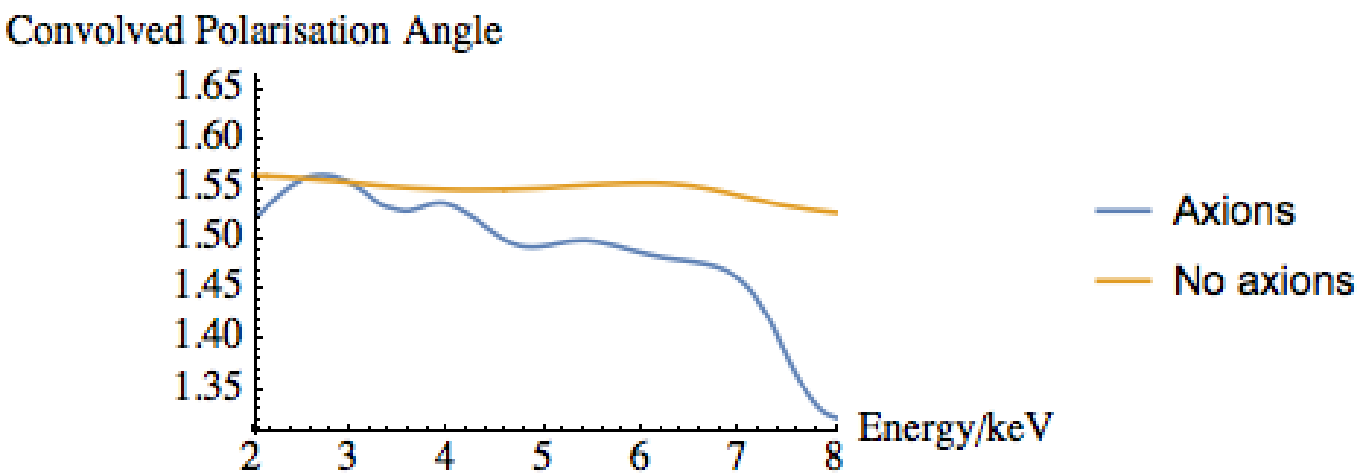

$$g_{a\gamma\gamma} = 3 \times 10^{-13}\,\mathrm{GeV}^{-1}$$

Type II AGN polarization

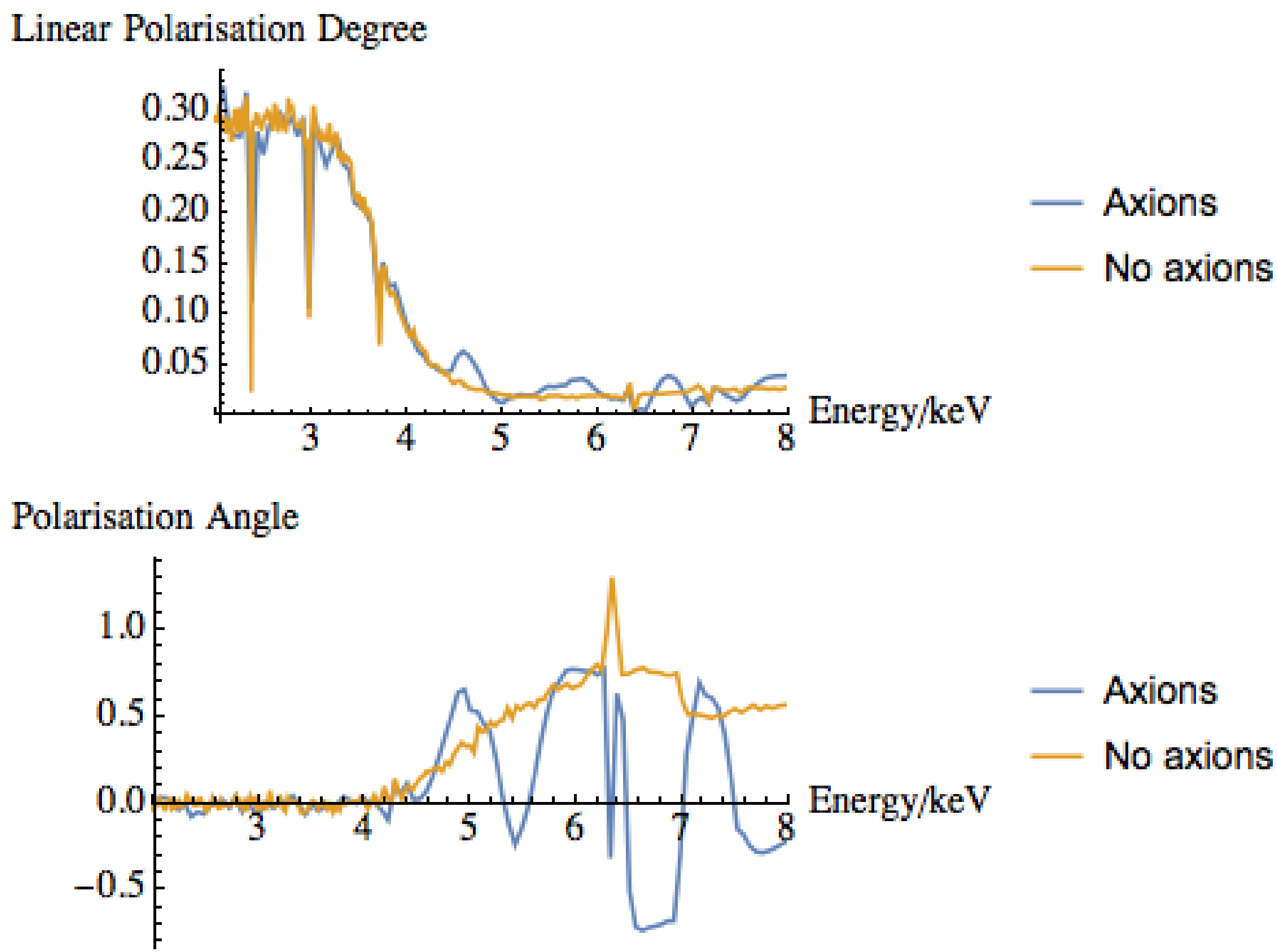

The linear polarization degree of a type-2 AGN in the absence (left) and presence (right) of axions.

Type II AGN polarization

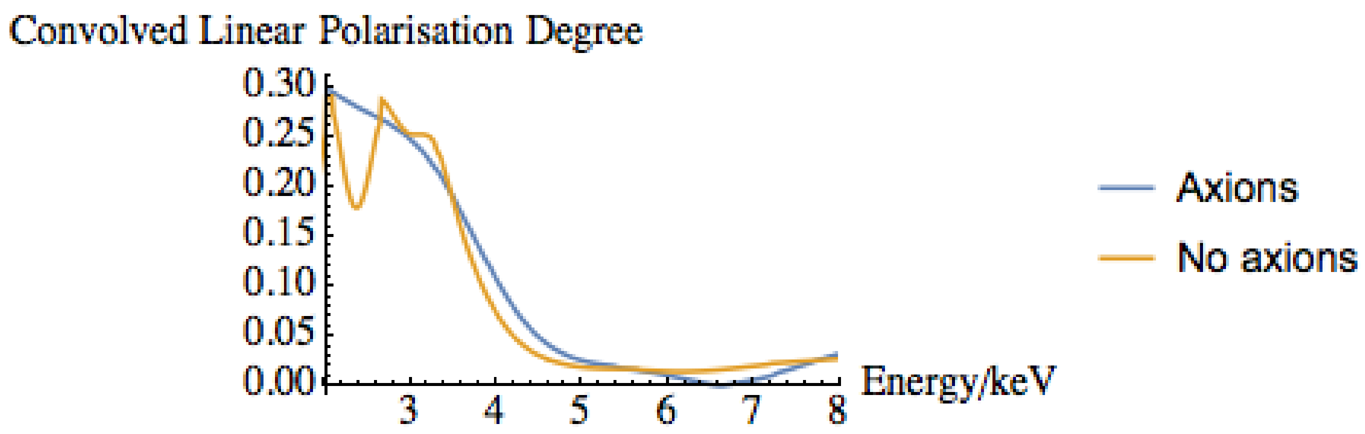

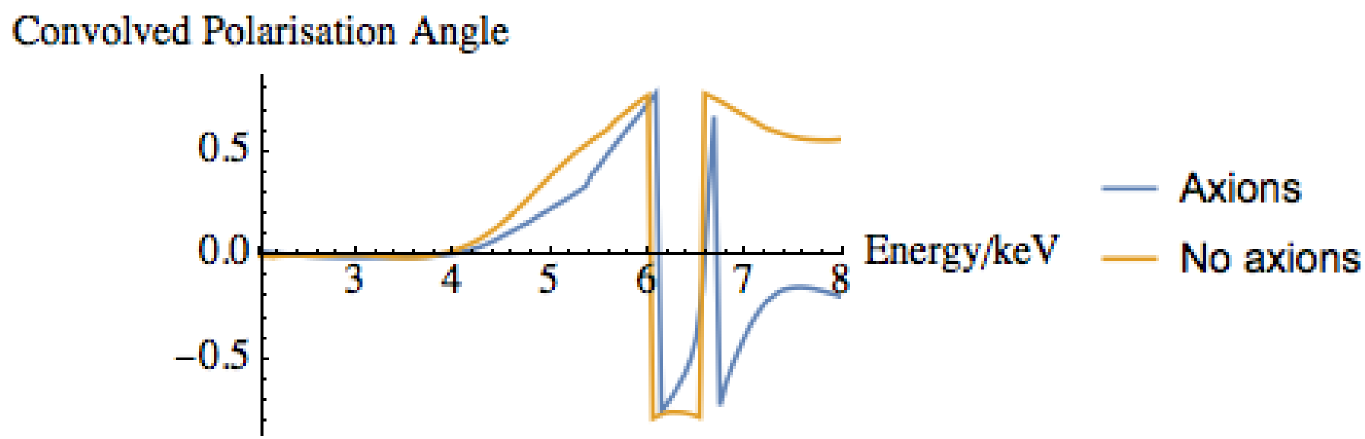

The linear polarization angle of a type-2 AGN in the absence (left) and presence (right) of axions.

Type I AGN Instrumental Modelling

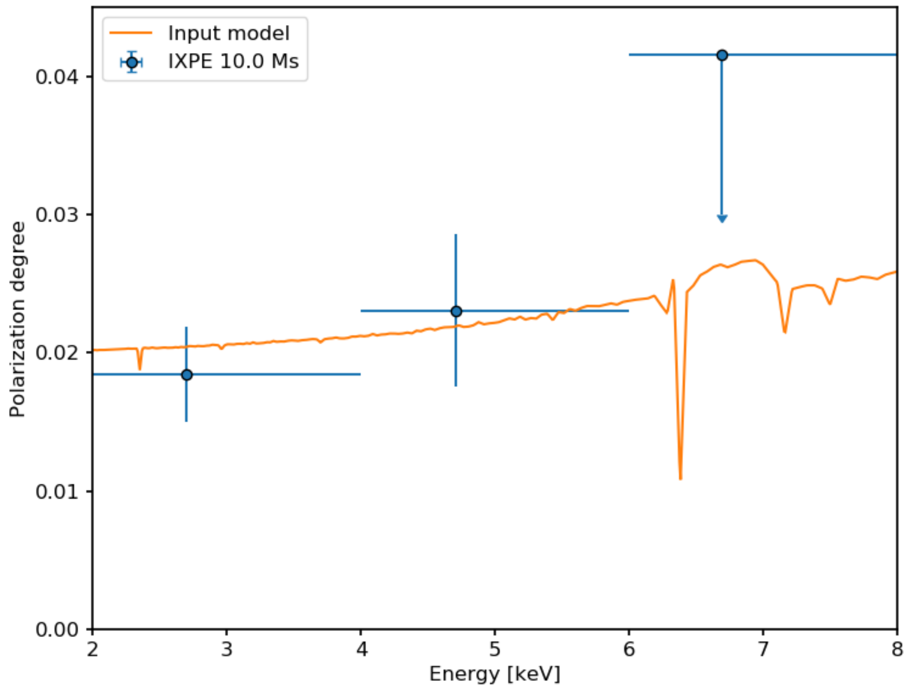

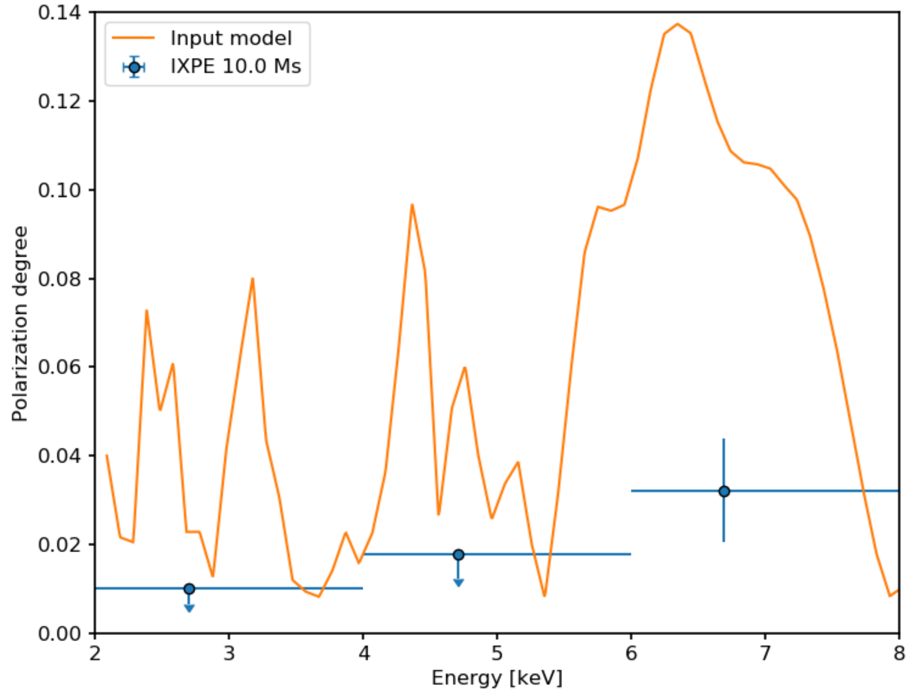

The linear polarization angle of a type-2 AGN in the absence (left) and presence (right) of axions.

Work in progress

Future directions

- Type 2 targets
- Other telescopes: enhanced X-ray Timing and Polarimetry Mission

Type I AGN Instrumental Modelling

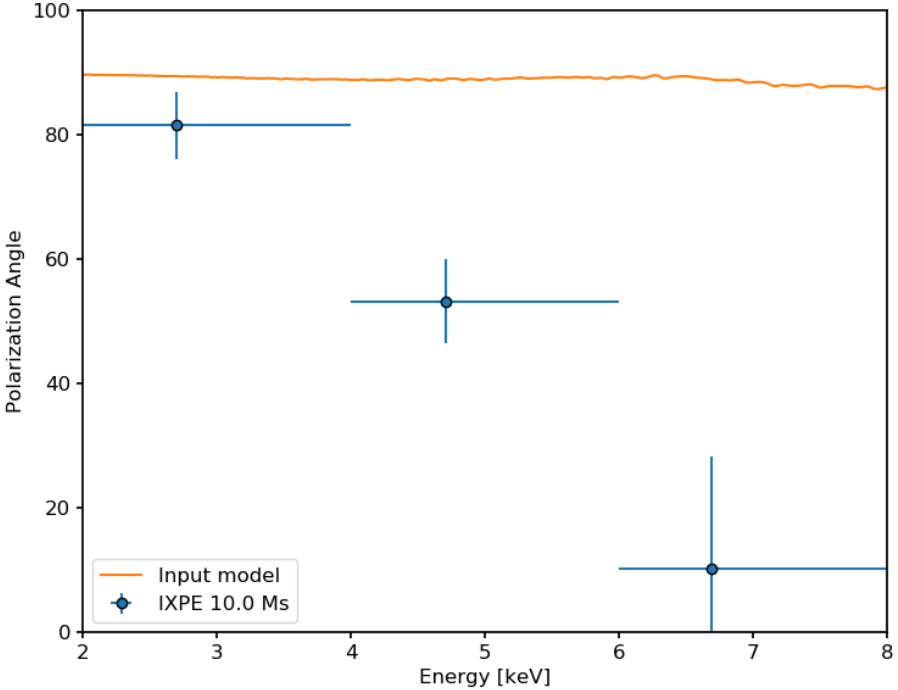

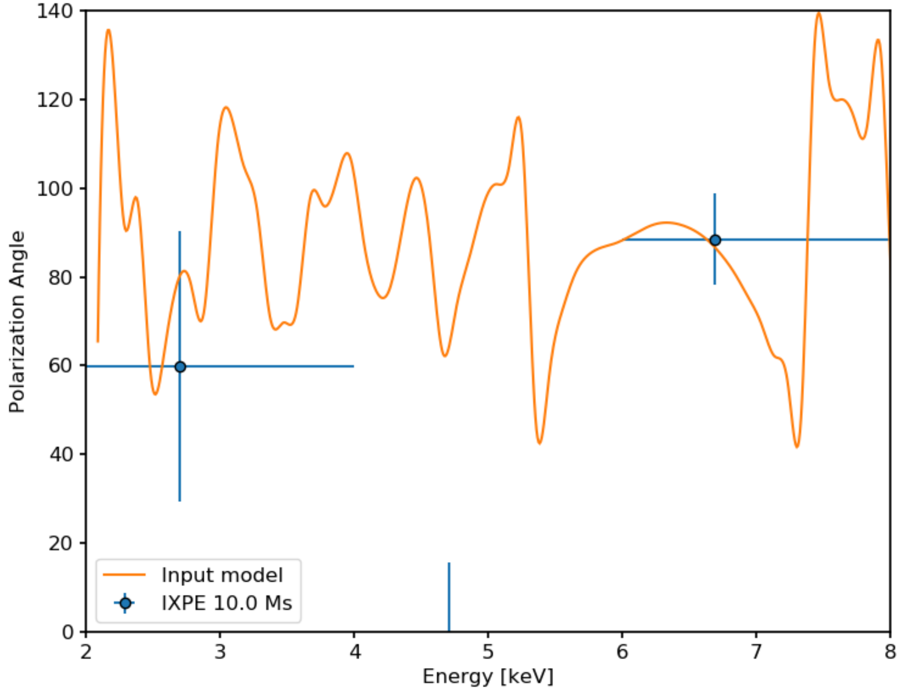

Bounds method 1

1. Randomly generate 1000 different magnetic field realisations $\mathbf{B}_i$ for the line of sight to NGC1275.
2. For each $\mathbf{B}_i$, generate the ALP induced linear polarisation $p_0^i(E)$ and polarisation angle $\psi_0^i(E)$ spectra, by numerically propagating the initial photon vector through the cluster.
3. From each $\{p_0^i(E), \psi_0^i(E)\}$ pair, generate 10 fake data sets.
4. Fit the no ALP constant model to each of the resulting 10,000 fake data sets, and find the corresponding likelihoods $\{L^i_{ga\gamma\gamma}\}$.
5. If fewer than 5% of the $\{L^i_{ga\gamma\gamma}\}$ are equal to or higher than $L^{\text{av}}_{\text{noALP}}$ (or L^{90}_{noALP} for the more pessimistic case), $g_{a\gamma\gamma}$ is excluded at the 95% confidence level.

Results 1

	0%	1%	5%
$L_{\mathrm{noALP}}^{\mathrm{av}}$	$1.2 \times 10^{-12}\,\mathrm{GeV}^{-1}$	$1.2 \times 10^{-12}\,\mathrm{GeV}^{-1}$	$6 \times 10^{-13}\,\mathrm{GeV}^{-1}$
L_{noALP}^{90}	$1.4 \times 10^{-12}\,\mathrm{GeV}^{-1}$	$1.3 \times 10^{-12}\,\mathrm{GeV}^{-1}$	$1.2 \times 10^{-12}\,\mathrm{GeV}^{-}$

Table: Projected upper limits on $g_{a\gamma\gamma}$ with IXPE. The columns correspond to different intrinsic polarisations of the AGN. The rows correspond to whether the average or 90th percentile likelihood value is used to characterize how well the no ALP model fits the simulated data.

Bounds method 2

- Follow *Fermi-LAT* (1603.06978)
- For each intrinsic source polarisation, simulate 1000 data sets $\{D_i\}$ with no ALPs present.
- Simulate transfer matrices for each value of g considered and for 100 different magnetic field configurations $\{B_j\}$.
- For each transfer matrix, find the final spectrum including ALPs for a range of different values for the intrinsic source polarisation degree $p_{\mathrm{lin}}^{\mathrm{source}}$ and angle ψ^{source}. We take $p_{\mathrm{lin}}^{\mathrm{source}} = 0 - 10\%$ in steps of 0.1% and $\psi^{\mathrm{source}} = 0 - \pi$ in steps of $\frac{\pi}{100}$, and we use an interpolating function derived from this data for the maximisation procedure later on.

Bounds method 2

- We now fit the spectra with ALPs generated in the previous step to the fake data generated without ALPs. For each set (g, B_j, D_i) we find the values of $p_{\rm lin}^{\rm source}$ and $\psi^{\rm source}$ that maximize the likelihood $L(g, B_j, p_{\rm lin}^{\rm source}, \psi^{\rm source} | D_i) = \prod_{\rm bins} L_k(g, B_j, p_{\rm lin}^{\rm source}, \psi^{\rm source} | D_i)$. In each bin k, L_k is the probability of measuring the $p_{\rm lin}$ and ψ values given by D_i, given that the true values are those predicted by an ALP model with parameters $(g, B_j, p_{\rm lin}^{\rm source}, \psi^{\rm source})$. These are calculated from Equation (3). We thus obtain a set of maximised likelihoods $L(g, B_j | D_i)$.

Bounds method 2

- For each value of g and each D_i, sort the $L(g, B_j|D_i)$ obtained from different magnetic fields, and select the 95th quantile L value, and the corresponding magnetic field. We thus obtain a set of likelihoods $L(g|D_i)$.
- For each D_i, find the value of g, $\hat{g}$ that leads to the maximum $L(g|D_i)$.
- We first consider the discovery potential of the data—i.e., the possibility of excluding a null hypothesis of no ALPs. For each D_i, we construct a test statistic $TS_i = -2\ln\left(\frac{L(g=0|D_i)}{L(g=\hat{g}|D_i)}\right)$.

Bounds method 2

- We have hence found the distribution of TS under a null hypothesis of no ALPs. We find the threshold TS value TS_{thresh} such that 95% of the TS_i are lower than TS_{thresh}. This value can be used to demonstrate our discovery potential for ALPs, by finding the TS for some of our fake data with ALPs included. We note that this test statistic does not obey Wilk's theorem as our hypotheses are not nested.
- We now turn to excluding values of g. Our null hypothesis is now that ALPs exist with some coupling g, and the alternative hypothesis H_1 is that $g \leq \hat{g}$. H_1 obviously includes the case where ALPs do not exist, but excluding ALPs with $g \leq \hat{g}$ should not be possible. Our test statistic for each g is now $\lambda(g, D_i) = -2\ln\left(\frac{L(g|D_i)}{L(\hat{g}|D_i)}\right)$.

Bounds Method 2

- We take the median value of $\lambda(g, D_i)$ over the D_i to represent that g. So we now have simply $\lambda(g)$ for our test statistic.
- We now need the null distribution of $\lambda(g)$ under the hypothesis that ALPs exist with coupling g. We assume that $\lambda(g)$ and the test statistic for a null hypothesis of no ALPs, TS above, have the same distribution, and therefore $\lambda(g)_{\text{thresh}} = TS_{\text{thresh}}$. We therefore exclude a value of g if $\lambda(g) > TS_{\text{thresh}}$.

Results 2

	0%	1%	5%
$L^{\mathrm{av}}_{\mathrm{noALP}}$	$6 \times 10^{-13}\,\mathrm{GeV}^{-1}$	$9 \times 10^{-13}\,\mathrm{GeV}^{-1}$	$1.3 \times 10^{-12}\,\mathrm{GeV}^{-1}$

Table: Projected upper limits on $g_{a\gamma\gamma}$ with IXPE using the likelihood ratio method. The columns correspond to different intrinsic polarisations of the AGN.